

## Article

# Thermal Simulations of Drilling of Cryogenic Lunar Soils Containing Water Ice

Jinsheng Cui <sup>1</sup>, Baoxian Chen <sup>1</sup>, Sibol Liu <sup>1</sup>, Deming Zhao <sup>2</sup> and Weiwei Zhang <sup>3,\*</sup>

<sup>1</sup> School of Mechanical and Electric Engineering, Guangzhou University, Guangzhou 510006, China; cuijinsheng86625@163.com (J.C.); chen861655598@163.com (B.C.); nc214618@163.com (S.L.)

<sup>2</sup> School of Mechanical Engineering, Zhejiang Sci-Tech University, Hangzhou 310018, China; zdm@zstu.edu.cn

<sup>3</sup> School of Mechatronics Engineering, Harbin Institute of Technology, Harbin 150001, China

\* Correspondence: zweier@hit.edu.cn

**Abstract:** Water ice is an important water source in lunar polar soil. Drilling and sampling lunar polar soil are important engineering tasks of lunar exploration. In view of the influence of temperature rise on the quality of samples obtained by drilling, the heat transfer and temperature rise in drilled ice-containing lunar soil were investigated. In this study, a thermal simulation model for drilling lunar soil was established based on the discrete element method (DEM). Simulations of the drilling temperature of lunar soil containing ice at 3–5% were performed assuming normal pressure and low temperature. After validating the feasibility and accuracy of the simulation method, the temperatures of the drilling tools and lunar soil were analyzed. Furthermore, drilling in a vacuum was simulated as well, and the results indicated that ice sublimation was negligible for reasonable drilling procedures in the current study.

**Keywords:** lunar exploration; thermal simulation; lunar soil; water ice; drilling; discrete element method (DEM)



**Citation:** Cui, J.; Chen, B.; Liu, S.; Zhao, D.; Zhang, W. Thermal Simulations of Drilling of Cryogenic Lunar Soils Containing Water Ice. *Aerospace* **2023**, *10*, 510. <https://doi.org/10.3390/aerospace10060510>

Academic Editor: Pierre Rochus

Received: 4 April 2023

Revised: 20 May 2023

Accepted: 26 May 2023

Published: 29 May 2023



**Copyright:** © 2023 by the authors. Licensee MDPI, Basel, Switzerland. This article is an open access article distributed under the terms and conditions of the Creative Commons Attribution (CC BY) license (<https://creativecommons.org/licenses/by/4.0/>).

## 1. Introduction

Extraterrestrial sampling, as the most direct way to explore extraterrestrial bodies, has played an extremely critical role and become the research focus of deep space exploration [1]. The Chinese Chang'e VII probe will be launched in 2026 to conduct environmental and resource exploration of the lunar South Pole. Drilling-based sampling, which requires a complicated soil–machine interaction coupling [2,3], is among the planned tasks. Research has been conducted on the thermal behavior of drilling-based sampling and soil particle systems. Zhang et al. [4–6] designed a new test bed and temperature measuring system to test the thermal performance of drilling in a lunar environment, and conducted experimental and theoretical research. Cui et al. [7,8] employed the discrete element method (DEM) to simulate the heat generation in lunar soil and rock drilling. Liu et al. [9] proposed a corresponding scheme to design a task operation mode and sampling machine for drilling frozen soil based on the analysis of the sampling environment and the objects in the polar region. In recent years, DEM has been widely used to study the heat transfer characteristics of discrete granular materials. Vargas and McCarthy [10,11] introduced the DEM contact heat transfer model, developed the dynamic hot particle method, and analyzed the heat transfer mechanism in particles. El Shamy et al. [12] simulated the contact heat conduction between particles using DEM, and the results also showed that the contact density affects the average thermal conductivity of the granular material. Chen et al. [13] established thermal DEM models of various materials with different particle sizes and derived a thermal contact theory to investigate the comprehensive heat transfer and effective thermal conductivity (ETC). Gong et al. [14] used a combination of DEM and dual-probability Brownian motion simulation to design a scheme to study the effects of particle shape, bulk density, and thickness on the ETC of granular materials. Lee et al. [15]

and Calvet et al. [16] combined DEM and finite elements to calculate the ETC of particles. Yan et al. [17] proposed a three-dimensional heat transfer model that considers contact heat transfer and thermal cracking in continuous–discontinuous media, combining DEM and finite elements. In addition, DEM also has been applied to solve problems encountered in extraterrestrial exploration, including lunar drilling. Li et al. [18] used DEM to calculate the ultimate uplift capacity of the anchor rod of the anchoring devices during the anchoring process for asteroid exploration. Wang et al. [19] studied the influence of ultrasonic drilling force–closure anchoring parameters on the anchoring performance for asteroid exploration based on DEM. Pelech et al. [20] determined the stability of small-diameter horizontal tunnels in lunar regolith and conditions using DEM. Pitcher et al. [21] performed DEM simulations for modelling dual-reciprocating drill interactions in regolith. Liang et al. [22] carried out a simulation using DEM to investigate the particle flow state of obstruction in Chang’e-5 drilling. Liu et al. [23,24] conducted in-depth research on kinematics, dynamics, and precision efficiency issues in lunar soil drilling based on DEM, verifying the applicability of DEM for lunar drilling issues.

Considering high-vacuum conditions, the low thermal conductivity of lunar soil, and inefficient auxiliary heat dissipation, drilling-based sampling may increase the samples’ temperature, thus affecting their properties. The thermal behavior of drilling cryogenic lunar soils containing water ice was investigated in this article. This article is organized as follows. In Section 2, we introduce the theoretical model of particle heat transfer that uses DEM, the extended particle–geometric heat transfer model, and the geometric heat transfer model that was developed in this work. Section 3 introduces the experimental setup, parameters, and results. Section 4 describes the simulation for experimental conditions, including DEM modeling, parameters, results, and analysis. Section 5 presents the model predictions for vacuum conditions, and Section 6 lists the conclusions of the present study.

## 2. Model

Soil can be regarded as an aggregate of particles, which are the building blocks of DEM. The heat transfer between particles in DEM can be parameterized as follows [10]:

$$Q_{ij} = 2k_s \left( \frac{3F_n r^*}{4E^*} \right)^{\frac{1}{3}} (T_j - T_i) \quad (1)$$

where  $i$  and  $j$  are the subscripts denoting the two interacting particles,  $Q_{ij}$  is the rate of the heat transfer from particle  $j$  to particle  $i$ ,  $k_s$  is the thermal conductivity of the respective granular material,  $F_n$  is the normal force between particles  $i$  and  $j$ ,  $E^*$  is the effective Young’s modulus given as  $E^* = \left( \frac{1-\nu_i^2}{E_i} + \frac{1-\nu_j^2}{E_j} \right)^{-1}$ ,  $r^*$  is the equivalent radius given as  $r^* = \frac{r_i r_j}{r_i + r_j}$ , and  $T_i$  and  $T_j$  are, respectively, the temperatures of particles  $i$  and  $j$ .

In general, the heat transfer between a pair of particles calculated using Equation (1) represents only the heat conduction between particles, while the convection and radiation modes are not considered. This approximation is justified by noting that the conductive mode most strongly determines the heat transfer between a pair of particles. On the other hand, a typical model in DEM is simplified by assuming the heat transfer between particles to be conductive; the resultant conduction is called effective heat conduction and is characterized by ETC. In the subsequent calibration of the particles’ parameters, our objective was to closely approximate the ETC of actual lunar soil with simulated particles. For a system of particles, the experimental thermal conductivity was ETC under the experimental conditions of the present study. In summary, considering the simplification and error of the model, the present study focused on ETC for investigating the heat transfer characteristics of granular matter assemblies.

In addition to particles as the building blocks, other physical entities in DEM are typically captured in terms of their geometry, such as the drilling tool in this study. In general, DEM does not involve the heat transfer model of a geometric body, and only uses

Equation (1) to calculate the heat transfer between particles. However, the DEM software typically provides an application programming interface (API). Using this API, users can write and compile custom models as user-defined libraries in C/C++.

Based on Equation (1), considering  $j$  as a geometric body, and regarding the geometric body as an infinite-radius particle ( $r_j \rightarrow \infty$ ), a particle–geometric heat conduction model was developed as follows:

$$Q_{ij} = 2k^* \left( \frac{3F_n r_s}{4E^*} \right)^{1/3} (T_j - T_i) \quad (2)$$

where  $k^*$  is the equivalent thermal conductivity given by  $k^* = \frac{2k_i k_j}{k_i + k_j}$ , and  $r_s$  is the particle radius.

In addition, based on the API, a heat transfer model for the drilling tool was developed. In the proposed model, the drilling tool was simplified as a one-dimensional object along the length; that is, the cross-sectional temperature of the drilling tool was considered to be uniform. On this basis, the one-dimensional drilling tool was divided into several infinitesimal elements (as described in Section 4.1), the heat conduction between each infinitesimal element was calculated using conventional numerical methods, and the convection or radiation of heat between the infinitesimal elements and the environment were considered. The entire process was considered from the viewpoint of energy. The energy transferred to the drilling tool, including kinetic energy imparted to the drilled soil, was eventually transformed into heat. Therefore, the heat source was mainly associated with rotational energy. The energy consumed by the feed and vibration was not considered, because its contribution was less than 1% of that of rotational energy. The heat source was summed and concentrated at the front of the drilling bit. The end of the drilling tool was considered an inclusion. A brief description of the heat transfer calculation process is shown in Figure 1.

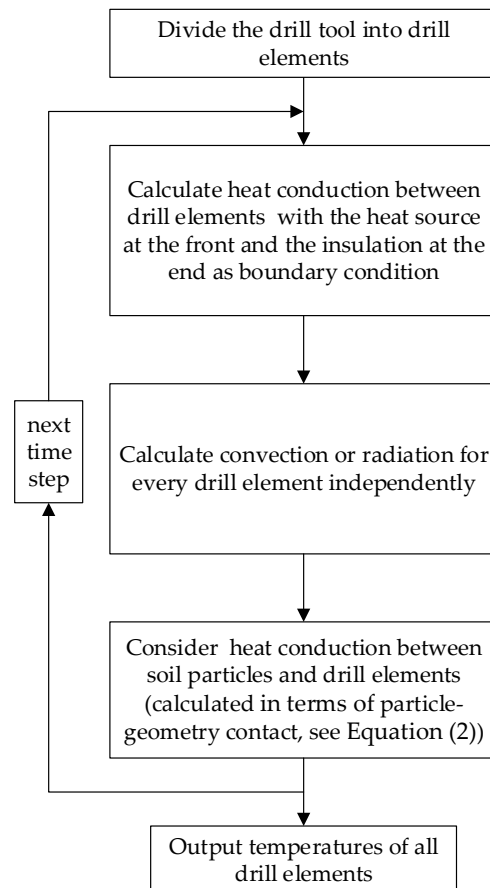


**Figure 1.** Brief description of the calculation of the heat transfer through the drilling tool.

### 3. Experiment

The drilling test bed is shown in Figure 2. It consisted of a mechanical system, a sensing system, and a sample. The feed movement was mainly guaranteed by weight-on-bit (WOB), with different WOBs obtained using the weight balance method. A rotary motor drove the drill bit to perform rotary motion. The test bed provided a vibration excitation device. A nitrogen environment sealing system was used to isolate the influence of external water vapor and reduce the ambient temperature, so as to simulate the actual working condition of drilling device rotary drilling on the lunar surface. The theoretical maximal drilling depth of the device was 300 mm. Temperature sensors were arranged in a cryogenic box to measure the environmental temperature field.

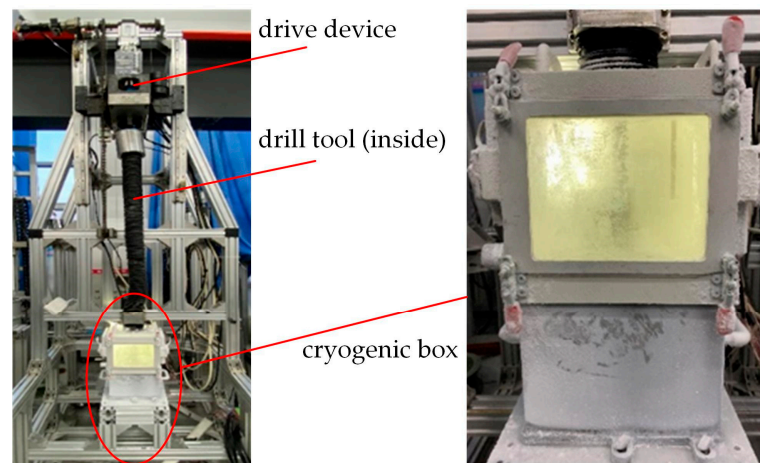


Figure 2. Drilling test bed.

The configuration and temperature measurement points (TMPs) of the drilling tool are shown in Figure 3. The length of the drilling tool was approximately 1 m, and the outer envelope diameter was 20 mm. The drilling tool was hollow, and the wall thickness was approximately 2–3 mm. During the test, the TMP readouts were collected simultaneously. The sampling mainly relied on the sampling part (the helical section was approximately 33.5 mm) close to the bit; that is, the lunar soil in the sampling helical section constituted the sample.

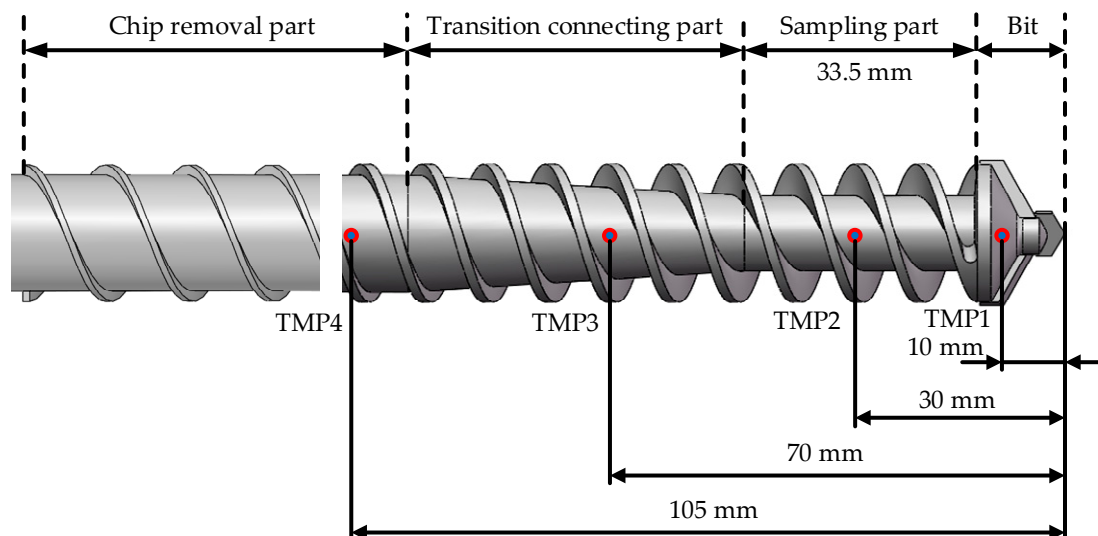


Figure 3. Drilling tool configuration and TMPs.

The water ice contents of the simulated lunar soil were 0% (dry soil), 3%, 4%, and 5% (considering the actual lunar polar water content prediction and engineering drilling ability). Dry soil was primarily used as a contrasting validation group to ensure the feasibility of the experiment and simulation. The composition of the simulated lunar soil water ice, the proportion of each component, the magnitude of particle size, and the proportion of particle size are shown in Table 1 below.

**Table 1.** The minerals, particle size range, and content of simulated lunar soil samples [25,26].

Mineral Class (Proportion)	Particle Size Range	Proportion
Anorthosite (70%)	0.025–0.05 mm	31.568%
	0.05–0.075 mm	6.797%
	0.075–0.1 mm	10.545%
	0.25–0.5 mm	10.545%
	0.5–1 mm	10.545%
Basalt (30%)	0.025–0.05 mm	13.502%
	0.05–0.075 mm	2.920%
	0.075–0.1 mm	4.526%
	0.25–0.5 mm	4.526%
	0.5–1 mm	4.526%

The preparation process of lunar soil water ice samples is as follows:

1. Weigh all kinds of particle sizes of anorthosite and basalt and place them in the oven for drying (more than 8 h);
2. According to the different materials' different particle size ratio configurations, put them into the blender for uniform mixing;
3. After the mixing of dry soil, the mixing of water into the samples should be allocated according to dry soil and different water content;
4. After the completion of mixed water configuration, leave the homogenized seal to stand for 6 to 8 h;
5. Use a press to compact the sample five times to the required compactness;
6. Sample the samples after compaction to verify the actual moisture content of the samples after preparation;
7. Transfer the samples to the secondary refrigeration freezer ( $-80\text{ }^{\circ}\text{C}$ ) for storage after 6–8 h of primary refrigeration ( $-30\text{ }^{\circ}\text{C}$ ). The samples need to undergo secondary refrigeration for 6–8 h before use.

The ETCs measured using the transient hot wire method in the range  $-180$ – $-170\text{ }^{\circ}\text{C}$  were  $0.209\text{ W/m}\cdot\text{K}$ ,  $0.554\text{ W/m}\cdot\text{K}$ ,  $0.677\text{ W/m}\cdot\text{K}$ , and  $0.861\text{ W/m}\cdot\text{K}$ , respectively. The simulated lunar soil and water can be mixed well in the container according to the required water content, and the initial pre-cooling can be carried out in a constant-temperature refrigerator. Then, a very low-temperature refrigeration device and evacuation equipment can be used to achieve the low temperature and vacuum conditions required for the experiment, and finally, the thermal conductivity can be calculated based on the experimentally measured parameters. During the drilling, the temperature sensors were placed in the simulated lunar soil, 25–45 mm away from the drilling center, to monitor the simulated lunar soil's temperature outside the drilling area. Owing to technical difficulties, the simulated lunar soil's temperature in the drilling area was not measured.

Drilling experiments were also conducted. The main experimental parameters are listed in Table 2, in which the first row lists the parameters controlling the feed rate, while the remaining rows list the parameters controlling the WOBs.

It should be noted that owing to the limitations of refrigeration technology, the temperature of the drilling tool and the space above the simulated lunar soil were not constant, but rather exhibited spatial gradients. The closer to the surface of the lunar soil, the lower

the temperature. In the follow-up simulations, the drilling tool and ambient temperature were fitted according to the corresponding measurement points.

**Table 2.** Experimental procedure parameters.

No.	Water Ice Content	Rotational Speed (rpm)	Feed Rate (mm/min)	WOB (N)	Impact Frequency (Hz)	Impact Energy (J)	Drilling Depth (mm)	Time (s)
1	0 wt%	120	50	–	0	0	100	120
2	3 wt%	120	98.4	190	5	2	100	61
3	4 wt%	120	58.3	190	5	2	100	103
4	5 wt%	120	25.0	190	5	2	100	240

The experimental torque and drilling tool's temperature are shown in Figure 4. The torque differences between the simulated lunar soils with water ice contents of 3%, 4%, and 5% were not significant, and were mainly owing to reasonable vibration excitation. Without vibration excitation, the torque associated with drilling lunar soils with higher water ice content was higher. However, Table 2 shows that there were still obvious differences between the corresponding footage speed values. Lunar soils with higher water ice content were more difficult to drill.

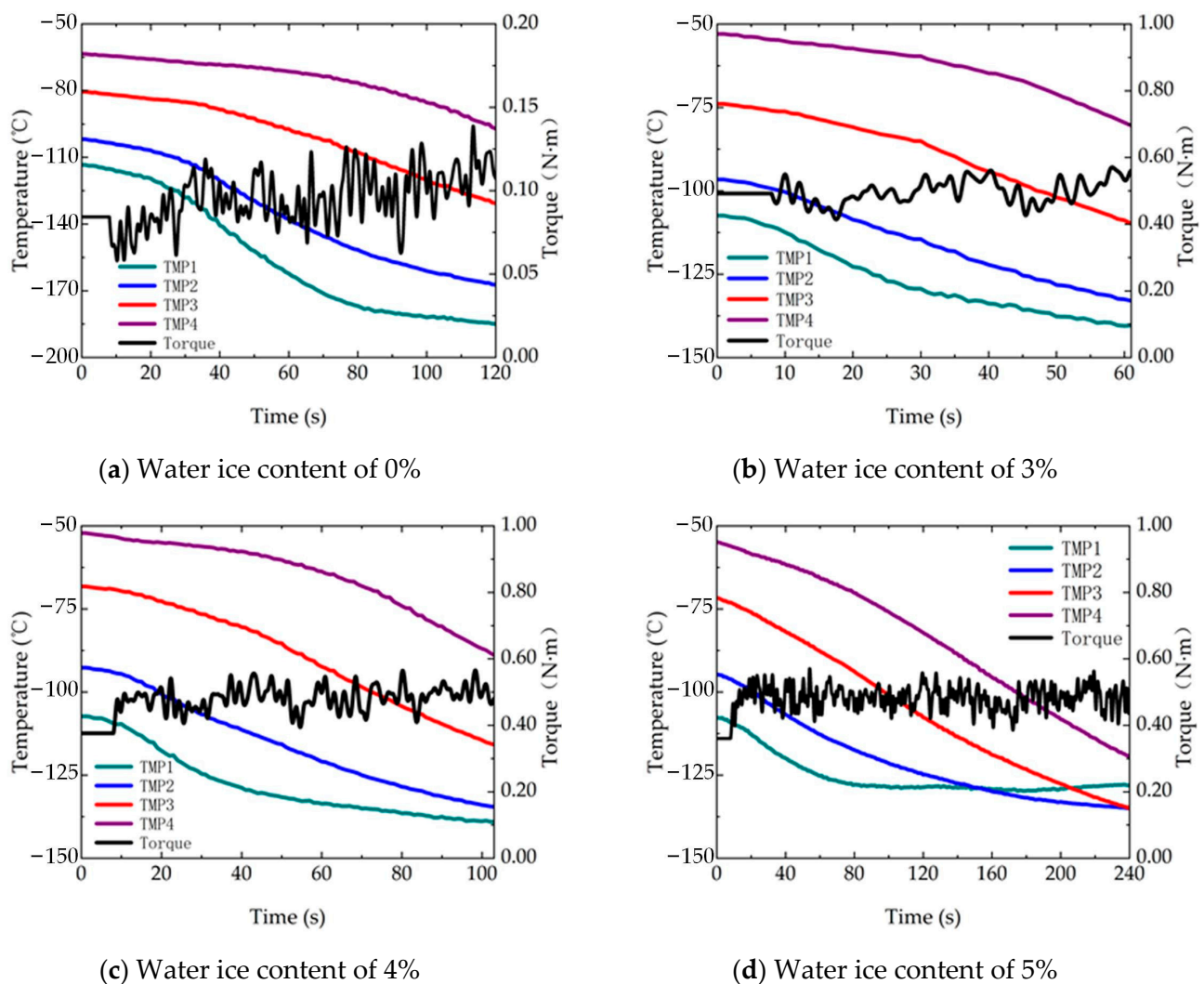


**Figure 4.** Experimental torque and drilling tool's temperature plots.

## 4. DEM Thermal Simulations Based on Experimental Conditions

### 4.1. DEM Model

The computational efficiency of DEM was affected by the model on one hand and the number of particles on the other hand. In general, the performance of most DEM simulations is constrained by the number of particles. Therefore, the lunar soil simulated using DEM in this study was established through the multistage amplification of particle sizes. As shown in Figure 5a, the general idea was filling the central zone with small particles, while filling the surrounding zone with large particles. Additionally, the multistage amplification of particle sizes reduced the number of particles on the premise of ensuring the highest possible level of accuracy. The diameter of the entire lunar soil sample was 70 mm, and the height was approximately 130 mm; this resulted from considering the boundary effect and computational complexity of the model.

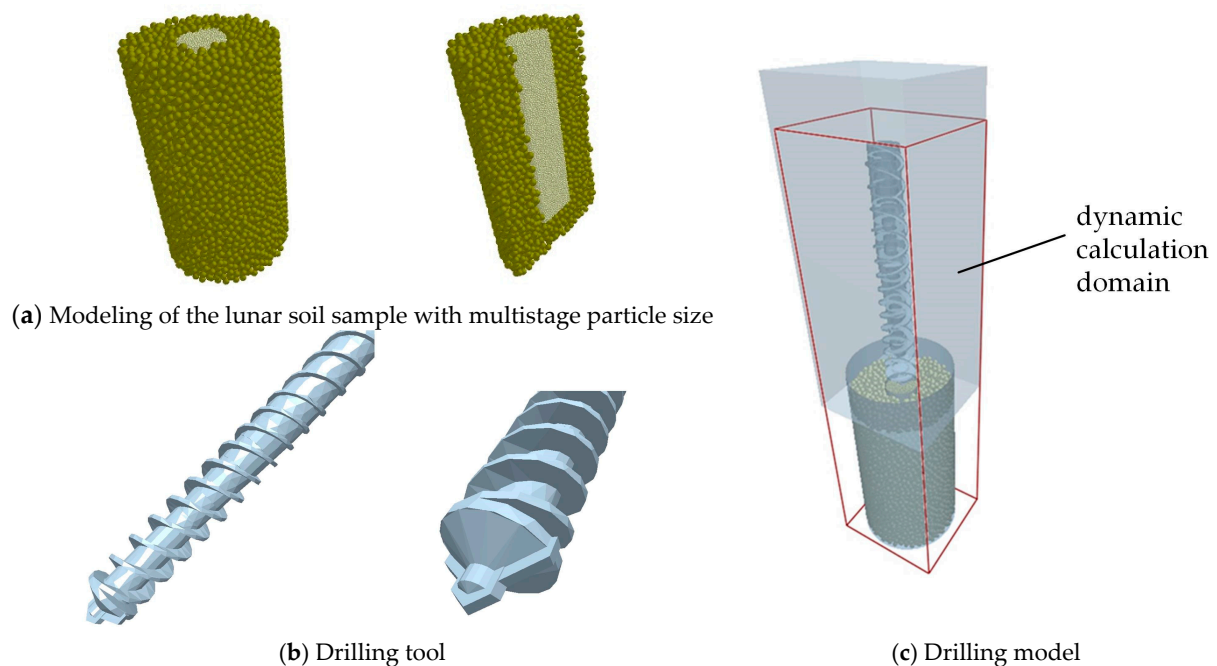


**Figure 5.** DEM model.

Owing to their complex geometry, drilling tools are typically modeled as three-dimensional objects, and the modeled objects are divided into equal-length infinitesimal elements as the basic units of numerical calculation, as described in Section 2. In the present study, all elements were at the same temperature. In this paper, the length of each individual element was 5 mm, while the length of the drilling tool was 1 m; thus, overall, there were 200 infinitesimal elements. It should be noted that such a division facilitated the temperature calculation, and the drilling tool moved or rotated as a single unit. In other words, there was no relative motion between any two elements. The drilling tool is shown in Figure 5b. The initial state of the DEM drilling model is shown in Figure 5c. The displayed length of the drilling tool in the simulation was approximately 150 mm.

To further increase the computational efficiency of the method, a dynamic computational domain was used in the simulation. Specifically, at the beginning of the simulation, the dynamic calculation domain was a translucent box, as shown in Figure 5c, which only contained lunar soil particles in the region approximately 15 mm below the drilling bit. The particles outside the dynamic calculation domain were not calculated temporarily (but were not deleted). The dynamic computation domain moved down with drilling and gradually increased the number of particles to be calculated, which significantly increased the calculation speed at the initial stage of the simulation, thus reducing the computation time of the entire simulation. One of the preconditions of this setting was that the particle

motion in this simulation was mainly concentrated the proximity of the drilling tool, and the heat transfer rate between the particles was relatively slow. Compared with the simulation results obtained without using the dynamic computational domain, the computation time was shorter by approximately 50–60%; at the same time, the results were not obviously different, and the maximal error was below 1%.

#### 4.2. Simulation Parameters

The simulation parameters are presented in Table 3.

**Table 3.** Parameters used in the simulation.

Parameters	Values
Particle thermal conductivity (W/m·K)	2.1/6.2/8.1/10.0 [27,28]
Particle specific heat (J/kg·°C)	200.0/257.5/277.7/297.9
Particle diameter (mm)	1.0/3.6
Number of particles	56,102
Particle density (kg/m <sup>3</sup> )	$3 \times 10^3$
Particle shear modulus (Pa)	$4 \times 10^7$
Particle Poisson's ratio	0.25
Geometry thermal conductivity (W/m·K)	12.7 (−100 °C) [29]
Geometry specific heat (J/kg·°C)	376 (−100 °C) [29]
Geometry density (kg/m <sup>3</sup> )	$7.85 \times 10^3$
Geometry shear modulus (Pa)	$8 \times 10^{10}$
Geometry Poisson's ratio	0.25
Friction coefficient between particles	0.48
Friction coefficient between particle and geometry	0.5
Drilling depth (mm)	100
Rotational speed (rpm)	120
Feed rate (mm/min)	50/98.4/58.3/25.0
Initial temperature (°C)	−196
Air convection coefficient (W/m <sup>2</sup> ·K)	25

In this study, the particles' thermal conductivity corresponded to the thermal conductivity of a single particle and not to the ETC of the system of particles. As mentioned in Section 2, this value was calibrated according to the measured ETC of the system of particles, that is, the simulated lunar soil. The calibration process used a central composite design (CCD) for optimization. The main steps of the parameter calibration process were as follows:

1. ETCs of the simulated lunar soil were measured. The measured values were the calibration targets.
2. The levels of the three factors (i.e., the three parameters that required calibration, specifically particle thermal conductivity, shear modulus, and diameter) were determined, and the CCD matrix was obtained.
3. DEM simulations were conducted to measure the ETC of the granular assembly according to the parameters in the CCD matrix.
4. The function describing the relationship between these factors and ETC was fitted using variance analysis based on the results of step 3.
5. The parameters that provided the fitting results closest to the calibration targets were determined via optimization. These parameters were used as the simulation parameters.

Similar optimization ideas for parameter calibration using orthogonal design have been widely used [27]. For a detailed description of this process, please refer to [28]. In addition, the particle diameter and shear modulus could be determined using this process.

It should be noted that the calibrated partial parameters were obtained using the calibration method. With these parameters, the ETCs of the modeled objects in DEM were similar to those in an actual system of objects. The purpose of the parameter calibration was not to develop particles that were the same as those in an actual granular assembly.

The model parameters did not represent the parameters of actual particles. Thus, some calibrated parameters were likely to differ significantly from those of actual materials. For example, the diameter of actual lunar soil particles is much smaller than the values that were used in our simulation. Owing to their larger diameter, the particles in DEM were approximately equivalent to the actual lunar soil particle clusters, and their shear modulus was far smaller than the actual one. Moreover, the larger particle size and smaller shear modulus were also conducive to more efficient calculations; thus, the computational complexity of the model was also considered when determining these two values. Our previous experience with parameter calibration was another important reason for determining the values of these two parameters.

The smaller of the two particle diameters in Table 3 was the result of parameter calibration. Based on the multistage amplification of the particle size mentioned in Section 4.1, small-diameter particles were used for modeling the central lunar soil, while large-diameter particles were used for modeling the peripheral lunar soil. The number of particles was one of the initial model parameters. It usually decreased slightly toward the end of the calculation, e.g., because individual particles moved out of the calculation domain. The particle specific heat was determined from the measured value, and the influence of temperature was considered. The variability intervals of density and Poisson's ratio were generally small; therefore, the common parameters of lunar soil were adopted. The properties of the geometry, that is, the drilling tools, were primarily based on those of stainless steel, and the geometric thermal conductivity and specific heat were estimated from fits, according to the results described in [29]. The friction coefficient was determined based on experience and known common values. The rotational speed, feed rate, and drilling depth were determined based on the experimental values. The convection coefficient was estimated according to the critical values of natural and forced convection.

In addition, as described in Section 3, the initial temperature fields of the drilling tools and environment, regarded as one-dimensional distributions, were fitted based on the measured values of the corresponding measurement points.

Sectional views of the drilling process are shown in Figure 6.

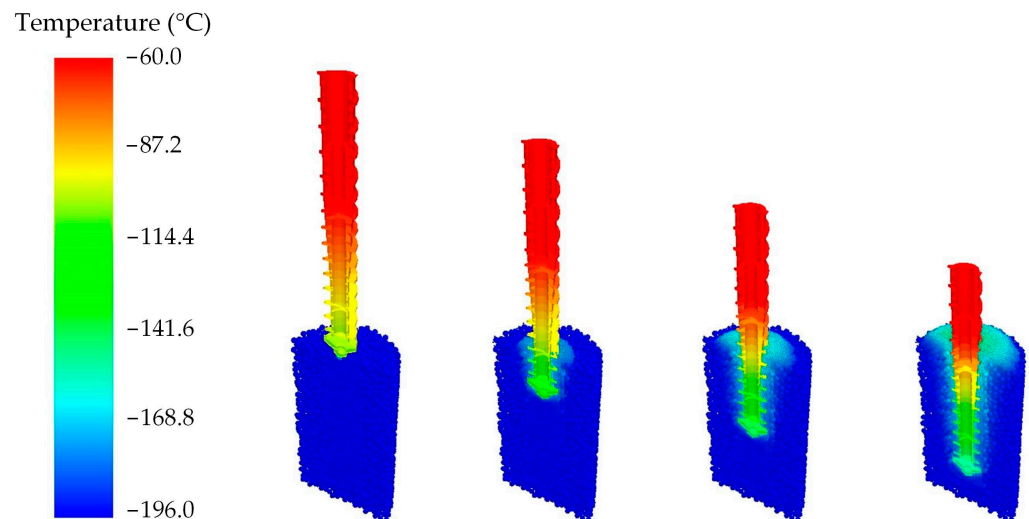


**Figure 6.** DEM thermal simulation of lunar soil simulant drilling based on experimental condition.

#### 4.3. Results and Analysis

The developed DEM model was used to conduct simulations for investigating the heat transfer characteristics during drilling, and for validating the feasibility of DEM. The simulated temperatures at the TMPs, which were the second, sixth, fourteenth, and twenty-first elements of the drilling tool, were compared with the experimental counterparts, as shown in Figure 7.

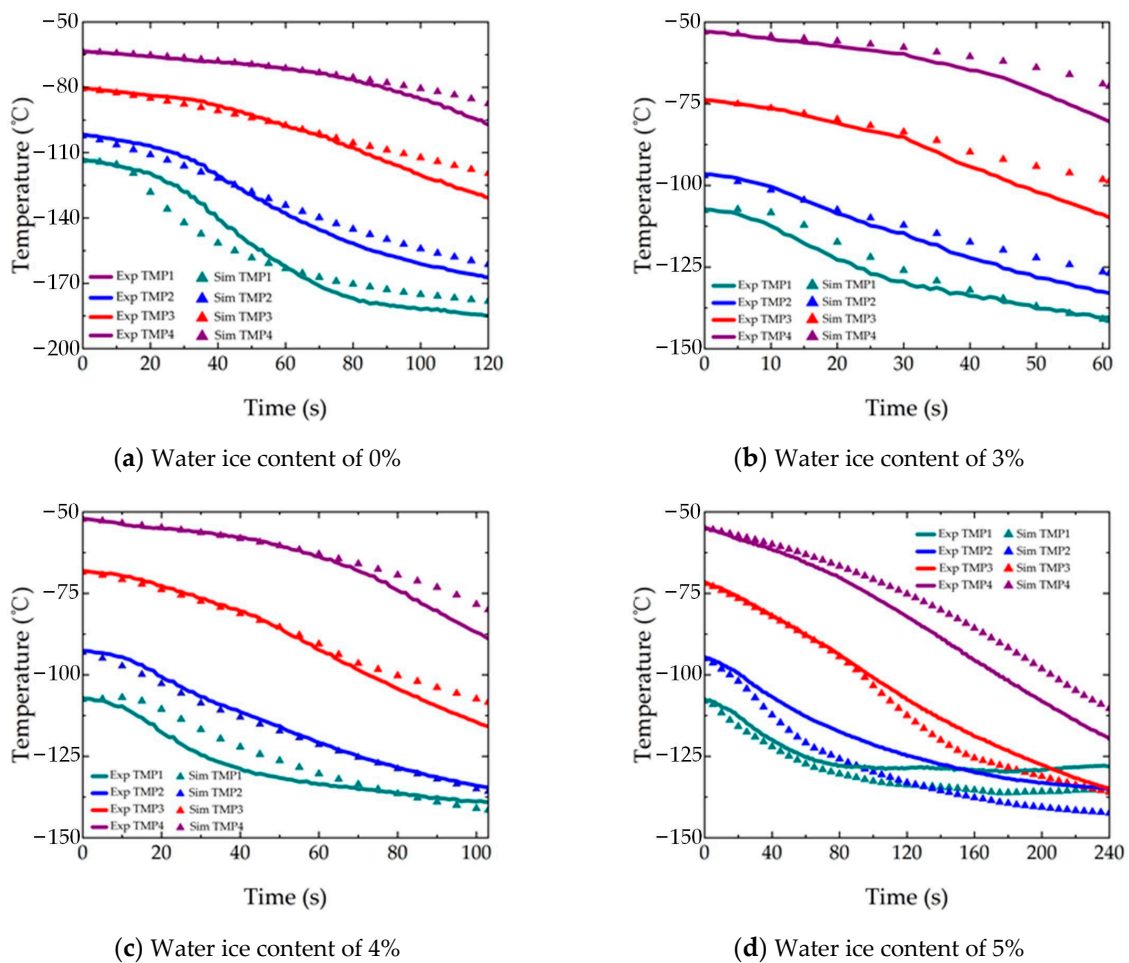


**Figure 7.** Comparison of the simulated and experimental TMP temperatures.

As can be seen from Figure 7a, the trends of the four TMPs in dry soil simulations were essentially similar to their experimental counterparts, and the maximal error was approximately 10 °C. In the early stage, the simulated temperature rise at the front of the drilling tool was lower than the experimental one, whereas in the later stage, the entire temperature rise was higher than the experimental one. The influence of the contact condition on the heat conduction between the drilling tool and lunar soil was not considered in the simulation. Therefore, the contact between the drilling tool (mainly the bit) and lunar soil was poor in the early stage of the drilling process. On the other hand, the contact clearly improved with continued drilling, the simulated lunar soil became compacted in the later stage of the drilling process, and the heat transfer between the drilling tool and lunar soil (particle–geometry) increased. However, this was not considered in the heat conduction model, which showed better heat conduction than in the actual situation during the early stage of the drilling process and worse heat conduction than in the actual situation during the later stage of the drilling process. The difference between the simulated and experimental TMP4 temperatures during the later stage of the drilling process was mainly due to the errors associated with the convection coefficient and ambient temperature field. This part of the drilling tool did not contact the lunar soil until the end of the drilling process.

It can also be seen from Figure 7b–d that the trends for the TMPs with the water ice content in the 3–5% range were essentially the same as those of the experimental results. The maximal error was observed at the front of the bit in the early stage of the drilling process, and at TMP4 in the later stage of the drilling process. The reason for the latter was similar to that for dry soil, whereas the former was primarily owing to the hypothesis of

the heat source in this simulation, which assumed that the heat source was concentrated at the bit. In the early stage of the simulation, all energy was converted into heat at the bit. The heat was transmitted to the bit and a very small number of particles in contact with the bit, which increased the bit's temperature. This was also reflected in the drilling of dry soil. However, the torque associated with the drilling of dry soil was very small; therefore, it was not obvious. Moreover, owing to the slow feed rate, the bit temperature in the scenario with the water ice content of 5% increased slightly in the later stage, but the overall temperature rise was lower than that in the scenario with the water ice content of 3–4%, indicating that lunar soil played a certain role in the heat dissipation by the drilling tool.

In addition, the errors of other parts of the drilling tool, including the sampling part, were small. This part was in contact with the sample, which was the primary concern, and the overall error was acceptable.

In summary, owing to the simplification of the model and inaccurate determination of some parameters, the simulation results had certain errors compared with the experimental results. However, the trends were essentially the same, and the degree of coincidence was high; therefore, the simulation was feasible and accurate. In addition, it was evident that the drilling tool was in a cooled state during the entire drilling process. The temperature of the drilling tool under various working conditions tended to be stable during the drilling. Drilling increased the temperature of the drilled lunar soil.

The final temperature fields obtained after drilling lunar soil samples with water ice contents in the 3–5% range are shown in Figure 8.

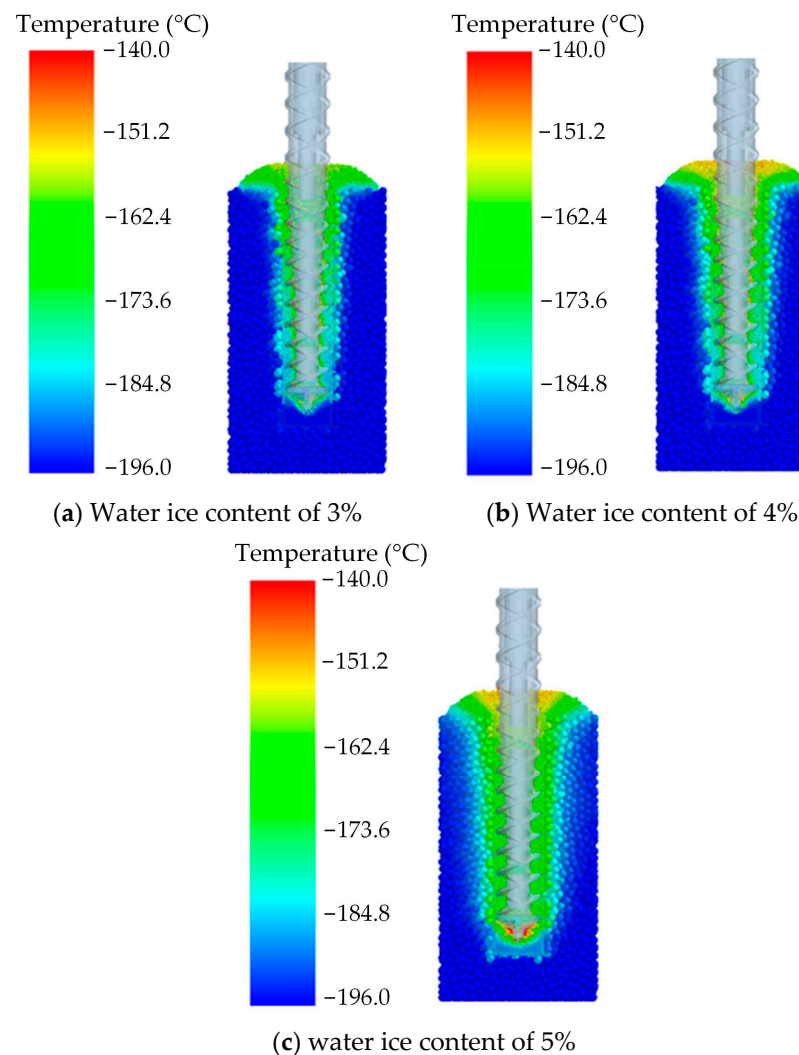


**Figure 8.** Temperature fields of lunar soil samples at the end of drilling.

As shown in Figure 8, owing to the drilling-induced heating, the temperature rise in the lunar soil systems was mainly concentrated in the proximity of the drilling pipe and bit, and the influence range was small. For most of the lunar soil, including the sampled area, the temperature was below  $-150\text{ }^{\circ}\text{C}$ . However, the temperature of some lunar soil near the drilling pipes, threads, and bits reached  $-140\text{ }^{\circ}\text{C}$ , and for a small number of particles in the case of the lunar soil samples with the water ice content of 5%, the temperature even reached  $-130\text{ }^{\circ}\text{C}$  (according to the data extracted from the simulations). The main reason for this was that the thermal conductivity of lunar soil was low, and heat could not be easily transferred. The temperature of lunar soil with the water ice content of 5% at the front of the bit was obvious, mainly owing to the high temperature of the bit.

In addition, it can be seen that the temperature of lunar soil discharged to the surface was higher, which was related to the approximation that omitted the impact of the surface convection in our simulations. This shows that lunar soil cooled the drilling tool and that some high-temperature lunar soil was transported upward, which had a certain heat dissipation effect on the drilling tool.

## 5. DEM Thermal Simulation in a Vacuum

### 5.1. Drilling Model and Parameter Modification in a Vacuum

In this section, drilling in a vacuum was simulated for lunar soils with the water ice contents of 3%, 4%, and 5%, and the temperatures of the drilling tool and lunar soil were predicted based on the experiment in Section 3 and the simulation in Section 4. In the vacuum, convection was ignored, and radiation from the drilling tool to the environment was added. In addition, the ETC of lunar soil decreased in the vacuum. According to the experimental measurements, the ETC values of simulated lunar soils with the water ice contents of 3%, 4%, and 5% were  $0.408\text{ W/m}\cdot\text{K}$ ,  $0.509\text{ W/m}\cdot\text{K}$ , and  $0.591\text{ W/m}\cdot\text{K}$ , respectively, which can be used as approximate estimates of the ETC values of actual lunar soils. Specifically, the estimated emissivity of the drilling tool was 0.24, assuming a smooth metal and considering the possibility of weak wear oxidation. The calibration results of the particles' thermal conductivity were  $4.5\text{ W/m}\cdot\text{K}$ ,  $5.6\text{ W/m}\cdot\text{K}$ , and  $6.9\text{ W/m}\cdot\text{K}$ , respectively. It should be noted that in the current plan, drilling was expected to be conducted in the shadow area, solar radiation was ignored, and the lunar soil temperature in the shadow area was low for a long time, which was similar to the experimental condition (in fact, it might be lower than the experimental one). Considering that high temperature was more unfavorable to the drilling process (for example, high temperature was more conducive to the water ice phase transition-mediated escape), it was more important to consider the experimental temperature of  $-196\text{ }^{\circ}\text{C}$  as the initial temperature.

### 5.2. Results and Analysis

After modifying the model, the drilling simulations of lunar soils with different water ice contents were performed according to the drilling parameters and load torque in the corresponding experiments. The simulation results of the TMPs and temperature fields are shown in Figures 9 and 10.

It can be seen from the figures that owing to the lower ECT values of lunar soil in the vacuum, the temperature at the front of the drilling tool was approximately  $10\text{--}20\text{ }^{\circ}\text{C}$  higher than that in the corresponding experiment (conducted at atmospheric pressure). On the other hand, the temperature of lunar soil in the vacuum reached  $-130\text{ }^{\circ}\text{C}$  (very few particles of lunar soil with the water ice content of 5% reached the temperature of  $-120\text{ }^{\circ}\text{C}$ ). The affected area and distribution of high-temperature lunar soil were similar to those obtained assuming atmospheric pressure. Analysis of the extracted data showed that the average temperature of lunar soil in the sampled area increased by approximately  $2\text{--}4\text{ }^{\circ}\text{C}$ , the maximal temperature increased by approximately  $6\text{--}8\text{ }^{\circ}\text{C}$ , and the temperature was essentially below  $-160\text{ }^{\circ}\text{C}$ . Considering that the ETC of lunar soil in the vacuum did not decrease significantly owing to the presence of water ice, this result was also in line with our expectations. Using the results of Formisano et al. [30], we estimated that the

water ice loss of lunar soil with the water ice content of 1 vol% after 10 min at  $-125\text{ }^{\circ}\text{C}$  was approximately 0.00023%, and for that at  $-100\text{ }^{\circ}\text{C}$ , it was approximately 0.095% (but when the temperature reached  $-50\text{ }^{\circ}\text{C}$ , the water ice would be completely lost within 10 min). As the proportion of water ice increased, this value continued to decrease. Based on this, the contribution of the water ice sublimation escape could be safely neglected in the present study. However, in reality, the effects of water ice evaporation during drilling are more complex and may affect, for example, the composition and ETC of lunar soils [31], which is a direction for follow-up research.

It should be noted that because of the experimental difficulty and time-consuming nature of the simulation, the drilling depth in this study was only 100 mm. However, the results of the drilling experiments and simulations suggest that for higher drilling depths, the temperature of the drilling tool and lunar soil will not change significantly (and will even tend to stabilize) if reasonable drilling procedures (rotational speed, footage force, and vibration excitation) can be ensured so that the torque or energy input will not change greatly. Changing the drilling target or drilling strategy (e.g., by increasing the water ice content, drilling into moon rock, or changing the drilling procedures) will invalidate the drilling strategy. This, in turn, may significantly increase the input energy or significantly decrease heat dissipation. Therefore, further analysis is required.

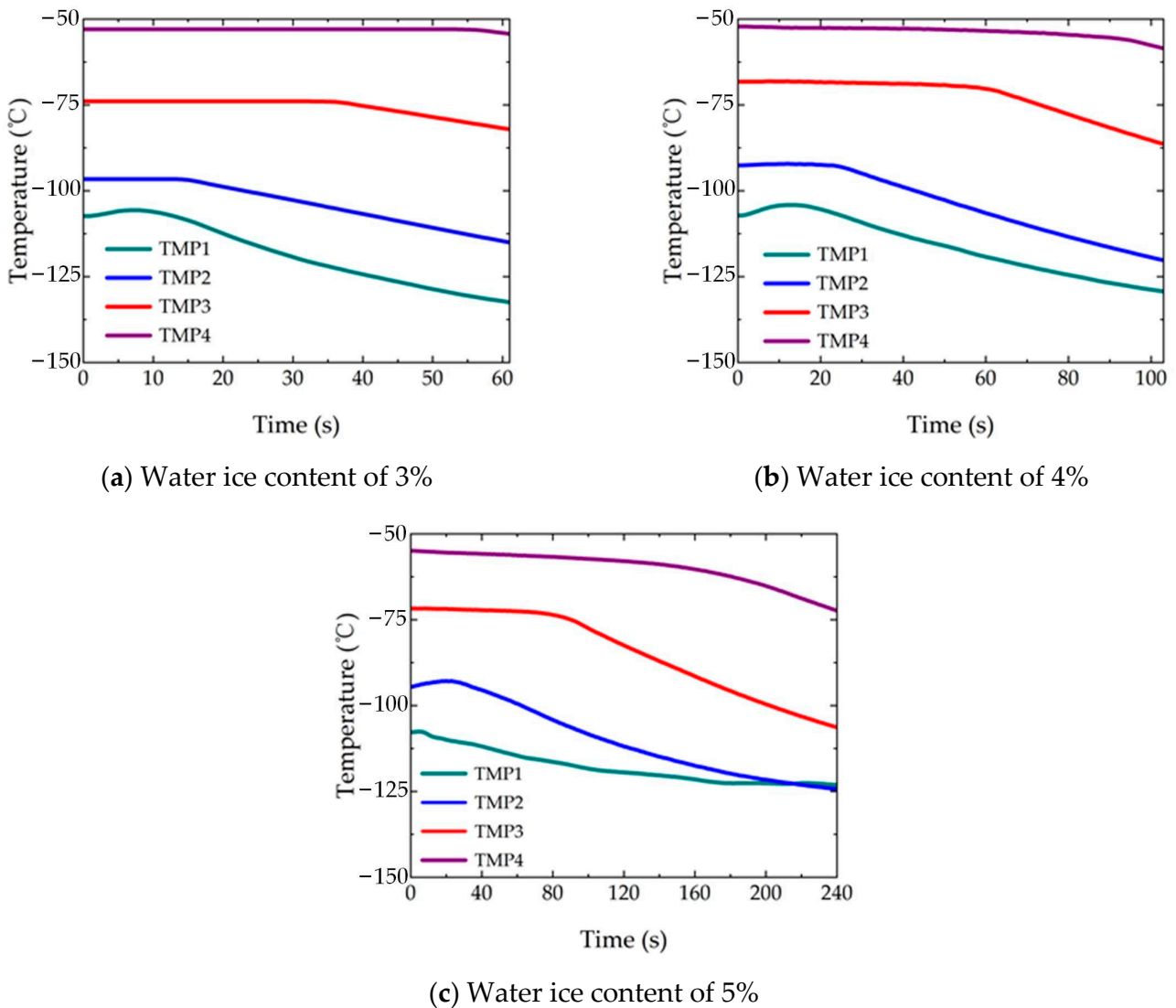
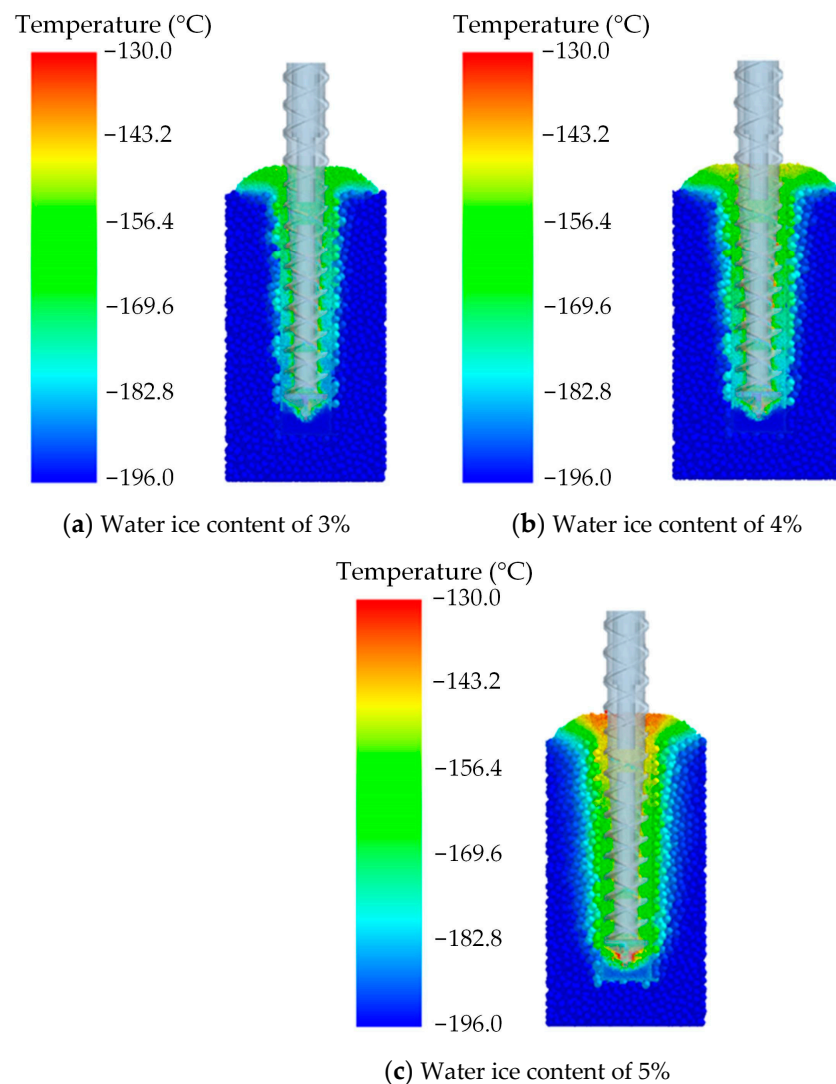


Figure 9. Simulation results of the TMPs drilling in vacuum.



**Figure 10.** Simulated temperature fields at the end of drilling in vacuum.

## 6. Conclusions

1. Using parameter calibration, a DEM heat transfer model for drilling cryogenic simulated lunar soil with water ice was established.
2. Cryogenic drilling experiments were carried out, and the drilling temperatures of dry soil and lunar soil with the water ice content in the 3–5% range in reasonable procedures assisted by vibration excitation were obtained.
3. The thermal simulation of drilling in cryogenic lunar soils with water ice was carried out, and the maximal error was approximately 10 °C, compared with the corresponding experimental results, validating the feasibility and accuracy of the DEM model. The results showed that lunar soil has an obvious cooling effect on the drilling tool, and the temperature of the drilling tool tended to stabilize with drilling. The temperature of lunar soil mainly increased near the drilling tool and during chip removal, which has a small influence range and was within an acceptable range.
4. By modifying the model, the drilling simulations of cryogenic lunar soils with water ice in a vacuum were carried out. The results indicated that for reasonable drilling procedures assumed in this paper, compared with the experimental results obtained at atmospheric pressure, the temperature of the drilling tool increased by approximately 10–20 °C, and the maximal temperature in the sampled area increased by approximately 6–8 °C. Furthermore, the contribution of the water ice sublimation-based escape could be safely neglected.

**Author Contributions:** Conceptualization, J.C.; methodology, J.C.; software, B.C. and S.L.; validation, D.Z. and W.Z.; writing—original draft preparation, J.C.; writing—review and editing, B.C., S.L., D.Z. and W.Z.; funding acquisition, J.C. and W.Z. All authors have read and agreed to the published version of the manuscript.

**Funding:** This research was funded by the National Natural Science Foundation of China, grant number 51705092 and the Science and Technology Program of Guangzhou, grant number 202102020320.

**Data Availability Statement:** Not applicable.

**Conflicts of Interest:** The authors declare no conflict of interest.

## References

1. Zhang, T.; Wang, B.; Wei, H.; Zhang, Y.; Chao, C.; Xu, K.; Ding, X.; Hou, X.; Zhao, Z. Review on planetary regolith-sampling technology. *Prog. Aerosp. Sci.* **2021**, *127*, 100760. [[CrossRef](#)]
2. Liu, T.X.; Zhou, J.; Liang, L.; Zhao, Y.; Cao, D.Q. Investigation of effect of stones on lunar regolith drilling using DEM. *Comput. Geotech.* **2021**, *131*, 103958. [[CrossRef](#)]
3. Tang, J.; Yang, T.; Chen, X.; Zhang, Z.; Tian, Y.; Zhang, W.; Jiang, S. Mechanical Characteristics of Lunar Regolith Drilling and Coring and Its Crawling Phenomenon: Analysis and Validation. *Aerospace* **2022**, *9*, 709. [[CrossRef](#)]
4. Zhang, T.; Zhao, Z.; Liu, S.T.; Li, J.L.; Ding, X.L.; Yin, S.; Wang, G.X.; Lai, X.M. Design and experimental performance verification of a thermal property test-bed for lunar drilling exploration. *Chin. J. Aeronaut.* **2016**, *29*, 1455–1468. [[CrossRef](#)]
5. Zhang, T.; Ding, X.L. A thermal model for predicting the drilling temperature in deep lunar regolith exploration. *Appl. Therm. Eng.* **2018**, *128*, 911–925. [[CrossRef](#)]
6. Zhang, T.; Ding, X.L.; Liu, S.T.; Xu, K.; Guan, Y.S. Experimental technique for the measurement of temperature generated in deep lunar regolith drilling. *Int. J. Heat Mass Transf.* **2019**, *129*, 671–680. [[CrossRef](#)]
7. Cui, J.S.; Hou, X.Y.; Wen, G.L.; Liang, Z.W. DEM thermal simulation of bit and object in drilling of lunar soil simulant. *Adv. Space Res.* **2018**, *62*, 967–975. [[CrossRef](#)]
8. Cui, J.S.; Hou, X.Y.; Wen, G.L.; Liang, Z.W. Thermal simulation of drilling into lunar rock simulant by discrete element method. *Acta Astronaut.* **2019**, *160*, 378–387. [[CrossRef](#)]
9. Liu, D.Y.; Zhang, H.; Yang, S.; Yin, C.; Zhang, J.B.; Sun, Q.C.; Lai, X.M. Lunar polar drilling sampling technique. *J. Deep Space Explor.* **2020**, *7*, 278–289. (In Chinese)
10. Vargas, W.L.; McCarthy, J.J. Stress effects on the conductivity of particulate beds. *Chem. Eng. Sci.* **2002**, *57*, 3119–3131. [[CrossRef](#)]
11. Vargas, W.L.; McCarthy, J.J. Thermal expansion effects and heat conduction in granular materials. *Phys. Rev. E* **2007**, *76*, 041301. [[CrossRef](#)] [[PubMed](#)]
12. El Shamy, U.; De Leon, O.; Wells, R. Discrete Element Method Study on Effect of Shear-Induced Anisotropy on Thermal Conductivity of Granular Soils. *Int. J. Geomech.* **2013**, *13*, 57–64. [[CrossRef](#)]
13. Chen, L.; Wang, C.; Moscardini, M.; Kamlah, M.; Liu, S.L. A DEM-based heat transfer model for the evaluation of effective thermal conductivity of packed beds filled with stagnant fluid: Thermal contact theory and numerical simulation. *Int. J. Heat Mass Transf.* **2019**, *132*, 331–346. [[CrossRef](#)]
14. Gong, Z.; Wu, Y.; Zhu, Z.G.; Wang, Y.; Liu, Z.Y.; Xu, W.X. DEM and dual-probability-Brownian motion scheme for thermal conductivity of multiphase granular materials with densely packed non-spherical particles and soft interphase networks. *Comput. Methods Appl. Mech. Eng.* **2020**, *372*, 113372. [[CrossRef](#)]
15. Lee, D.; Pham, K.; Kang, M.; Park, S.; Choi, H. Stepwise DE/FE combined approach for estimating effective thermal conductivity of frozen spherical particulate media. *Comput. Geotech.* **2020**, *128*, 103837. [[CrossRef](#)]
16. Calvet, T.; Vanson, J.M.; Masson, R. A DEM/FFT approach to simulate the effective thermal conductivity of granular media. *Int. J. Therm. Sci.* **2022**, *172*, 107339. [[CrossRef](#)]
17. Yan, C.Z.; Wei, D.S.; Wang, G. Three-dimensional finite discrete element-based contact heat transfer model considering thermal cracking in continuous-discontinuous media. *Comput. Methods Appl. Mech. Eng.* **2022**, *388*, 114228. [[CrossRef](#)]
18. Li, M.X.; Tang, D.W.; Quan, Q.Q.; Zhao, Z.J.; Guo, F.; Meng, L.Z.; Deng, Z.Q. Investigation on the ultimate uplift capacity for asteroid exploration in drilling anchoring process: Numerical modelling and DEM simulation. *Adv. Space Res.* **2021**, *67*, 3026–3036. [[CrossRef](#)]
19. Wang, T.Z.; Quan, Q.Q.; Xu, Y.; Yu, H.Y.; Tang, D.W.; Deng, Z.Q. Study the influence of anchoring parameters on asteroid drilling anchoring with discrete element simulation. *Adv. Space Res.* **2023**, *71*, 816–828. [[CrossRef](#)]
20. Pelech, T.; Barnett, N.; Dello-Iacovo, M.; Oh, J.; Saydam, S. Analysis of the stability of micro-tunnels in lunar regolith with the Discrete Element Method. *Acta Astronaut.* **2022**, *196*, 1–12. [[CrossRef](#)]
21. Pitcher, C.; Alkalla, M.; Pang, X.; Gao, Y. Development of the Third Generation of the Dual-Reciprocating Drill. *Biomimetics* **2020**, *5*, 38. [[CrossRef](#)] [[PubMed](#)]
22. Liang, J.N.; Tao, L.J.; Zhang, W.W.; Tang, J.Y.; Pang, Y.; Jiang, S.Y. Analysis of the lunar regolith sample obstruction in the Chang'E-5 drill and its improvement. *Adv. Space Res.* **2022**, *69*, 2248–2258. [[CrossRef](#)]

23. Liu, T.X.; Liang, L.; Zhao, Y.; Cao, D.Q. Equivalent boundary model of lunar soil drilling simulation by DEM. *J. Terramechanics* **2020**, *91*, 85–95. [[CrossRef](#)]
24. Liu, T.X.; Zhou, J.; Liang, L.; Bai, Z.F.; Zhao, Y. Effect of drill bit structure on sample collecting of lunar soil drilling. *Adv. Space Res.* **2021**, *68*, 134–152. [[CrossRef](#)]
25. Cui, J.; Kui, L.; Zhang, W.; Zhao, D.; Chang, J. Simulation of Drilling Temperature Rise in Frozen Soil of Lunar Polar Region Based on Discrete Element Theory. *Aerospace* **2023**, *10*, 368. [[CrossRef](#)]
26. Zhao, D.; Cheng, Z.; Zhang, W.; Cui, J.; Wang, H. Numerical Modeling of Thermal Behavior during Lunar Soil Drilling. *Aerospace* **2023**, *10*, 472. [[CrossRef](#)]
27. Wang, X.W.; Ma, H.Z.; Li, B.; Li, T.J.; Xia, R.; Bao, Q.B. Review on the research of contact parameters calibration of particle system. *J. Mech. Sci. Technol.* **2022**, *36*, 1363–1378. [[CrossRef](#)]
28. Deng, Z.Q.; Cui, J.S.; Hou, X.Y.; Jiang, S.Y. Calibration of Discrete Element Heat Transfer Parameters by Central Composite Design. *Chin. J. Mech. Eng.* **2017**, *30*, 419–427. [[CrossRef](#)]
29. Gupta, A.; Kavakbasi, B.T.; Dutta, B.; Grabowski, B.; Peterlechner, M.; Hickel, T.; Divinski, S.V.; Wilde, G.; Neugebauer, J. Low-temperature features in the heat capacity of unary metals and intermetallics for the example of bulk aluminum and Al<sub>3</sub>Sc. *Phys. Rev. B* **2017**, *95*, 094307. [[CrossRef](#)]
30. Formisano, M.; De Sanctis, M.C.; De Angelis, S.; Carpenter, J.D.; Sefton-Nash, E. PROSPECTING the Moon: Numerical simulations of temperature and sublimation rate of a cylindrical sample. *Planet. Space Sci.* **2019**, *169*, 8–14. [[CrossRef](#)]
31. Metzger, P.T.; Zacny, K.; Morrison, P. Thermal Extraction of Volatiles from Lunar and Asteroid Regolith in Axisymmetric Cranka-Nicolson Modeling. *J. Aerosp. Eng.* **2020**, *33*, 04020075. [[CrossRef](#)]

**Disclaimer/Publisher's Note:** The statements, opinions and data contained in all publications are solely those of the individual author(s) and contributor(s) and not of MDPI and/or the editor(s). MDPI and/or the editor(s) disclaim responsibility for any injury to people or property resulting from any ideas, methods, instructions or products referred to in the content.